Structural Engineering and Mechanics, Vol. 8, No. 5 (1999) 465-476
DOI: http://dx.doi.org/10.12989/sem.1999.8.5.465

Optimum design of parabolic and circular arches with varying cross section

Umit Uzman† and Ayse Daloglu‡

Department of Civil Engineering, Karadeniz Technical University, 61080 Trabzon, Turkey

M. Polat Saka‡†

Department of Civil Engineering, University of Bahrain, Bahrain

Abstract. A structural optimization process is presented for arches with varying cross-section. The optimality criteria method is used to develop a recursive relationship for the design variables considering displacement, stresses and minimum depth constraints. The depth at the crown and at the support are taken as design variables first. Then the approach is extended by taking the depth values of each joint as design variable. The curved beam element of constant cross section is used to model the parabolic and circular arches with varying cross section. A number of design examples are presented to demonstrate the application of the method.

Key words: optimization of arches; arch bridges; curved beams; circular arch element; parabolic arch element.

1. Introduction

Arches are one of the earliest structures used by man in the history. They are curved structures that provide economical solutions for crossing large spans. Compared with beams smaller cross sections can be used in arches as the axial forces are dominant. Further economy can be achieved in the design of these structures by using structural optimization. Large number of optimum design algorithms exist in the literature which minimize the weight or the cost of the structure while satisfying the strength and serviceability limitations Haftka, Gurdal and Kamat (1990). Some of these algorithms obtain the optimum topology of a structure in addition to finding the optimal cross sectional properties, Ding (1986). Tadjbakhsh (1981) developed an algorithm which determines the optimum profile of an arch considering the stability constraints. Bensalem, Sibbald and Fairfield (1998) presented an optimum design approach for arch bridges based on their modal characteristics. They found that ultimate capacities of arches are related to their resonant frequencies.

The purpose of this paper is to develop an algorithm for the optimum design of arch structures

† Associate Professor
‡ Assistant Professor
‡† Professor

with uniform and/or varying cross section subjected to displacement, stress and side constraints. In the formulation of the design problem the depths at the supports and at the crown are treated as design variables while the width of the cross section is taken constant. The arch is divided into number of elements and average depth of each element is also treated as additional design variable. With the inclusion of displacement and stress constraints the design problem turns out to be nonlinear programming. The optimality criteria method is employed to obtain its solution which was reported to be quite effective in solving nonlinear optimum design problems by No and Aguinalde (1987), Saka and Hayalioglu (1991) and Saka and Hayalioglu (1991) and Saka and Ulker (1992).

The optimum design algorithm presented computes three different values for each design variable in every design cycle depending on the dominance of the type of the constraints. The first one is computed from the recursive relationship which is obtained by employing the optimality criteria that is constructed for the case of dominant displacement constraints. The second one is calculated from the stress constraints. The third value for the depth variable is specified by the minimum size constraints. The largest of these three values defines the new values of the design variables for the next step. This procedure is continued until convergence is achieved.

The design procedure presented here is straightforward which provides very easy programming and locates the optimum design of the arches with uniform and varying cross-section under the displacement, stress and minimum depth constraints.

2. Analysis of arches

An arch element under end forces is shown in Fig 1a and 1b. The relationship between the end forces and the displacements for such an element may be written as

$$\{P\} = [K]\{u\} \tag{1}$$

Where,

$$\{P\} = \{P_1\, Q_1\, M_1\, P_2\, Q_2\, M_2\}^T \tag{2}$$

and

$$\{u\} = \{u_1\, v_1\, \varphi_1\, u_2\, v_2\, \varphi_2\}^T \tag{3}$$

$[K]$ is the stiffness matrix, given in Marquis and Wang (1989) for a parabolic arch element with

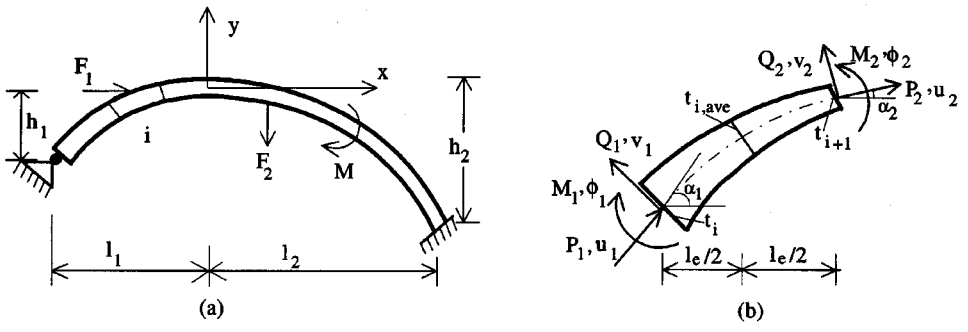

Fig. 1 a) Arch, b) Finite segment with end forces

constant cross section using the force method. The circular arch element of constant cross section is used for the optimum design of circular arches. Readers can refer to Arbabi (1991) and Cook, Malkus and Plesha (1989) for more details. Both stiffness matrices are not presented here since the expressions are too lengthy to repeat.

After evaluating the axial force, shear force and bending moment values at each point, normal and shear stresses at any section can be calculated as:

$$\sigma = \frac{N}{bt} + \frac{6M}{bt^2} \leq \sigma_{al} \tag{4}$$

$$\tau = \frac{3}{2}\frac{T}{bt} \leq \tau_{al} \tag{5}$$

since $t \ll R$, where R is the radius of curvature. σ_{al} and τ_{al} show the allowable normal and shear stresses.

3. Objective function and constraints

The objective is to minimize the weight of the arch by reducing the depth of the cross section. However, there may be some limitations on the displacements and rotations to consider while the optimum depth of the cross section is searched. Hence, there is an objective such as the minimization of the weight of the arch to find the optimum values of the depths, and there are some restrictions like the upper bounds of the displacements and the stresses, and also the lower bound of the depths.

The depths at the nodes are determined by solving the optimization problem. Several cases are considered in this study. The variation of the depth along the arch can be expressed as a function of x

$$t = t(x) \tag{6}$$

in terms of some other parameters such as d_i, i=1, ..., nd (Figs. 2a, b, c, d). The average depth of each element can also be calculated by inserting the x value of the middle section of the related segment into Eq. (6).

$$x_{i,ave} = \frac{x_i + x_{i+1}}{2}, \qquad t_{i,ave} = t(x_{i,ave}) \tag{7}$$

The cases considered in the study are as follows:

a) The depth is assumed to be constant along the arch (Fig. 2a),

$$t(x) = d_1 \tag{8}$$

which means there is only one design variable d_1, mainly nd=1, and $t_{i,ave}=d_1$ in each segment which is obtained by Eq. (7).

b) The variation of the depth is assumed to be linear along the arch (Fig. 2b),

$$t(x) = A + Bx \tag{9}$$

where,

$$A = \frac{1}{l_1 + l_2}(l_2 d_1 + l_1 d_2)$$

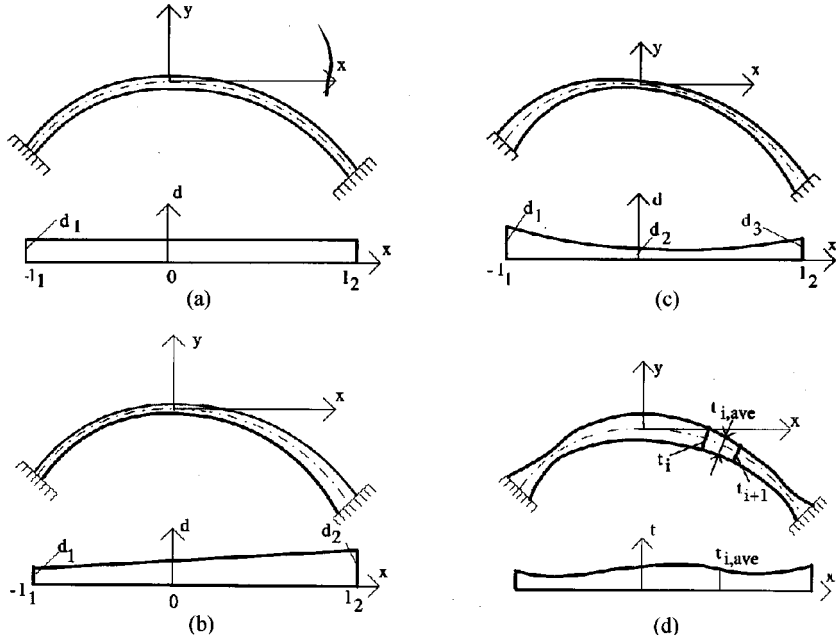

Fig. 2 Variation of depth along arch

$$B = \frac{1}{l_1 + l_2}(-d_1 + d_2)$$

The number of the design variables *nd* is equal to two: d_1, d_2 and *nd*=2 which are the depths of the left and right supports of the arch.

c) The depth is assumed to be a parabolic function of x along the arch (Fig. 2c),

$$t(x) = A + Bx + Cx^2 \tag{10}$$

where,

$$A = d_2$$

$$B = \frac{1}{l_1 + l_2}\left[-\frac{l_2}{l_1}d_1 + \left(\frac{l_2}{l_1} - \frac{l_1}{l_2}\right)d_2 + \frac{l_1}{l_2}d_3\right]$$

$$C = \frac{1}{l_1 + l_2}\left[\frac{1}{l_1}d_1 + \left(-\frac{1}{l_1} - \frac{1}{l_2}\right)d_2 + \frac{1}{l_2}d_3\right]$$

The number of design variables *nd* is equal to three, d_1, d_2, d_3 which are the depths at the left support, at the crown and at the right support of the arch. After the design variables are obtained, the value of the depth at each node is calculated by inserting the x value of the related node into the expressions (8), (9) or (10) for cases (a), (b), and (c).

d) The variation of the depth for each finite segment is assumed to be linear and depths at the joints are calculated independent of each other (Fig. 2d). Hence, the number of design variables is equal to the number of joints, *nd*=*nj*=*nm*+1.

$$d_i = t_i, \qquad i = 1, ..., nd$$

$$t(x) = d_i + \frac{d_{i+1} - d_i}{x_{i+1} - x_i}(x - x_i) \qquad x_i \le x \le x_{i+1}, \qquad i = 1, 2, ..., nm$$

The design variables are determined by solving the optimization problem. The average depth of a related element is then determined by linear interpolation or by Eq. (7) as follows:

$$t_{i,ave} = \frac{t_i + t_{i+1}}{2} \qquad i = 1, ..., nm \tag{11}$$

4. Optimality criteria approach

As mentioned before, the problem to be solved is to minimize the total weight of an arch with displacement, stress and minimum depth constraints. It is assumed that the arch is divided into *nm* elements.

The weight of such an arch can be defined as

$$W = \sum_{i=1}^{nm} \rho\, b t_{i,ave}\, l_i \tag{12}$$

where, ρ is the density of the material, *nm* is the number of elements, $t_{i,ave}$ is the average thickness, W is the total weight of the structure, l_i and b are the length and the width of the element, respectively.

The displacements, stresses and limit values of the depth are the constraints in the optimization process. These constraints can be formulated as:

$$g_j = \Delta_j - \Delta_{ju} \le 0 \qquad j = 1, ..., p \tag{13}$$

$$t_i - t_{il} > 0 \qquad i = 1, ..., nj \tag{14}$$

$$\sigma \le \sigma_{al}, \quad \tau \le \tau_{al} \qquad i = 1, ..., nj \tag{15}$$

where Δ_j is the displacement of joint j and Δ_{ju} is its upper bound, p is the number of restricted displacements, σ_{al}, τ_{al} are allowed equivalent normal and shear stresses at the ith element, σ *ve* τ are the actual equivalent stresses at the same element, and t_{il} is the lower bound on the design variable t_i. The associated Lagrangian function of this problem is expressed as

$$L(d_k, \lambda_j) = \sum_{i=1}^{nm} b\ \rho\, l_i t_{i,ave} + \sum_{j=1}^{p} \lambda_j g_j \tag{16}$$

and the optimality conditions become

$$\frac{\partial L}{\partial d_k} = \sum_{i=1}^{nm} \rho\, b l_i c_{ik} + \sum_{j=1}^{p} \lambda_j \frac{\partial g_j}{\partial d_k} = 0 \tag{17}$$

where,

$$c_{ik} = \frac{\partial t_{i,ave}}{\partial d_k}, \qquad k = 1, ..., nd \tag{18}$$

The values of c_{ik} will be different for each case mentioned in section 3. That is,

Case a) for constant variation of the depth, single design variable, d_1, using Eqs. (7), (8) and (18), one can obtain

$$c_{i1} = 1, \qquad i = 1, ..., nm \tag{19a}$$

Case b) for the linear variation of the depth, two design variables of d_1 and d_2, using Eqs. (7), (9) and (18), one can obtain

$$\begin{aligned} c_{i1} &= \frac{1}{l_1 + l_2}(l_2 - x_{i,ave}) \\ & \qquad\qquad i = 1, ..., nm \\ c_{i2} &= \frac{1}{l_1 + l_2}(l_1 + x_{i,ave}) \end{aligned} \tag{19b}$$

Case c) for parabolic variation of the depth, three design variables d_1, d_2 and d_3, using (7), (10) and (18), one can obtain

$$\begin{aligned} c_{i1} &= \frac{1}{(l_1 + l_2)\, l_1}(-l_2 x_{i,ave} + x_{i,ave}^2) \\ c_{i3} &= \frac{1}{(l_1 + l_2)\, l_2}(+l_1 x_{i,ave} - x_{i,ave}^2) \qquad i = 1, ..., nm \\ c_{i2} &= 1 - c_{i1} - c_{i3} \end{aligned} \tag{19c}$$

Case d) Finally, for any variation of the depth, nj design variables t_i, using Eqs. (11) and (18), one can obtain

$$c_{ik} = \begin{cases} 1/2 & k{=}i \quad \text{or} \quad k{=}i{+}1 \\ 0 & k{\neq}i \quad \text{and} \quad k{\neq}i{+}1 \end{cases} \qquad i = 1, ..., nm \tag{19d}$$

Inserting Eq. (13) into the second term of Eq. (17) yields:

$$\frac{\partial g_j}{\partial d_k} = \frac{\partial \Delta_j}{\partial d_k} \tag{20}$$

Then, by using the virtual work method, the jth displacement can be expressed as

$$\Delta_j = \sum_{i=1}^{nm} \{X^e\}_i^T [k]_i \{X^v\}_{ij} = \sum_{i=1}^{nm} \frac{f_{ij}}{t_{i,ave}^3} \tag{21}$$

where f_{ij} is called the flexibility coefficient which is given as

$$f_{ij} = t_{i,ave}^3 \{X^e\}_i^T [k]_i \{X^v\}_{ij} \tag{22}$$

nm is the total number of members. $\{X^e\}_i$ are the end joint displacements of member i due to external loads, $[k]_i$ is the stiffness matrix of the ith member, $\{X^v\}_{ij}$ is the end joint displacements of the member due to unit loading applied in the direction of restricted displacement j, and $t_{i,ave}$ is the average thickness of the member i. The bending effect in thin members is dominant compared to those of the normal and shear forces. This effect is inversely proportional with $t_{i,ave}^3$ because the bending rigidity, EI, is in the denominator. Noticing this, the displacement expression is described

by dividing f_{ij} by $t_{i,ave}^3$ instead of $t_{i,ave}$. Hence, f_{ij} must be multiplied by $t_{i,ave}^3$.

Substituting Eq. (21) into the constraint equality of Eq. (13) and taking the derivative with respect to d_k yields

$$\frac{\partial g_j}{\partial d_k} = -\sum_{i=1}^{nm} \frac{3f_{ij}}{t_{i,ave}^4} \frac{\partial t_{i,ave}}{\partial d_k} = -\sum_{i=1}^{nm} \frac{3f_{ij}}{t_{i,ave}^4} c_{ik} \tag{23}$$

Hence, the optimality criteria are obtained by substituting Eq. (23) into Eq. (17),

$$\frac{3\sum_{j=1}^{p} \lambda_j \sum_{i=1}^{nm} \frac{f_{ij}\, c_{ik}}{t_{i,ave}^4}}{\sum_{i=1}^{nm} \rho b l_i c_{ik}} = 1 \qquad k = 1, ..., nd \tag{24}$$

This expression is transformed into an iterative one so that it can be used to obtain the new values of variables at every design cycle. This is achieved by multiplying both sides by d_k^r and then taking the rth root

$$d_k^{v+1} = d_k^v \left[\frac{3\sum_{j=1}^{p} \lambda_j \sum_{i=1}^{nm} \frac{f_{ij}\, c_{ik}}{t_{i,ave}^4}}{\sum_{i=1}^{nm} \rho b l_i c_{ik}} \right]^{1/r} \qquad k = 1, ..., nd \tag{25}$$

where v is the current and v+1 is the next optimum design cycle. r is known as the step size and its value is preselected before starting the design process. The value of $1/r$ is selected as 0.5 in the design example. Refer to Hayalioglu and Saka (1992) for more information.

It can be noticed from Eq. (25) that the use of above equation requires the values of Lagrange multipliers to be known. One of the methods to select it is to take the constraint equality in Eq. (13) and to multiply both sides by λ_j^c and to take the cth root. This leads to the following recursive relationship:

$$\lambda_j^{v+1} = \lambda_j^v (\Delta_j / \Delta_{ju})^{1/c} \qquad j = 1, ..., p \tag{26}$$

where c is called the step size. In this study $1/c$ is selected as 0.75. Refer to Saka and Ulker (1992), Saka and Hayalioglu (1991), No and Aguinagalde (1987) for more explanation. The initial values of the Lagrange multipliers must be selected in order to use this equation.

5. Design examples

As mentioned before, parabolic and circular arches are considered, and there are few cases for the variation of the depths along the arches. The concentrated moments and forces are applied at the nodes.

Before presenting results for a problem, a convergence study is thought to be of use to the reader. The convergence study is done for both fixed and hinged supported arches as illustrated in Fig. 3. Different numbers of elements are used for the analysis, and the weight of the arch is plotted with respect to the number of elements. It is observed that 16 finite elements are

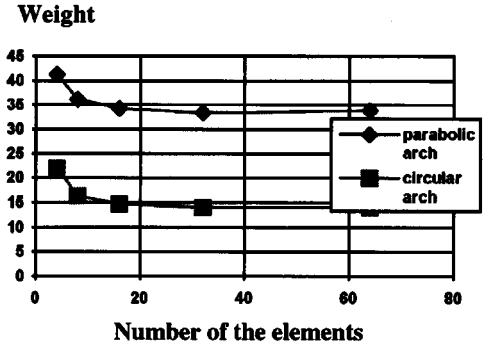

Fig. 3 Convergence study for parabolic and circular arches

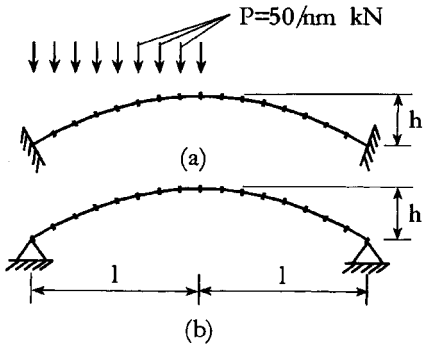

Fig. 4 Parabolic arch, l=10 m, h=1, 2.5, 5m (nm is the number of elements)

reasonable for the examples considered here. The weight of the arch and the depth of the elements have not been changed considerably when more than 16 elements are used.

The following examples are chosen to investigate all these situations and to show how the optimization process works. The modulus of elasticity of the material and the allowable stress are taken as 20700 kN/cm^2 and 25.20 kN/cm^2, respectively, for all the design examples. The width of the cross section is constant at b=10 cm. Only the depth varies along the arch, and this is not allowed to be less than a lower bound, t_u=2.5 cm. The supports are fixed (Fig. 4a) or hinged (Fig. 4b). As a last example, a parabolic arch shown in Fig. 10 is considered under two displacement constraints. The initial value of the Lagrange multipliers is taken as 5 in the design examples. The number of elements is chosen as 16 for all the examples.

5.1. Parabolic arch under loads at half span

The depths along the arch are computed for three different values of the arch height and different variations of the depths as shown in Fig. 2. The vertical displacement of the node at l/4

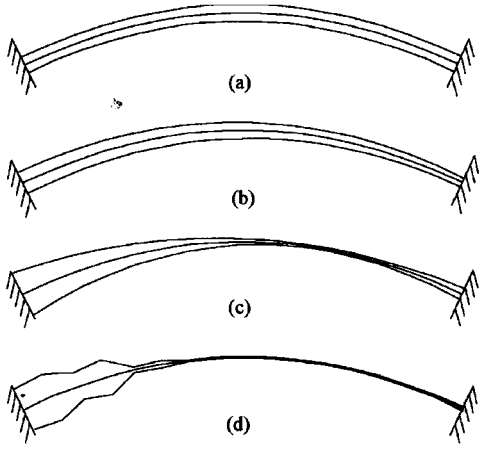

Fig. 5 Variation of the depth along a clamped parabolic arch

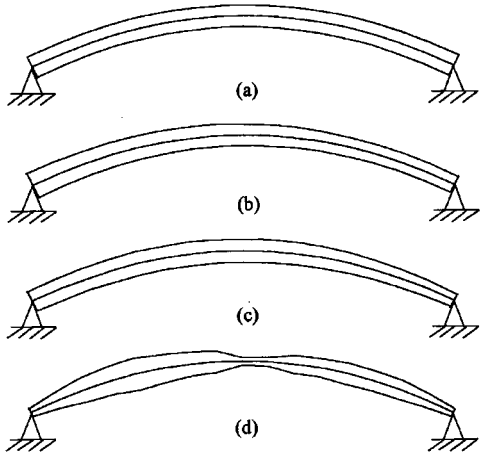

Fig. 6 Variation of the depth along a hinged parabolic arch

Table 1 Results for clamped parabolic arch

Case	h(m)	ite.no	W (kN)	Design variables d_i (cm), i=1, ..., nd								
a	1	12	32.1752	20.7								
	2.5	11	32.2323	20.1								
	5	11	36.7296	20.8								
b	1	11	30.0709	29.5	9.2							
	2.5	10	30.9628	27.7	10.8							
	5	10	35.5013	28.2	11.8							
c	1	13	25.6581	57.5	6.9	13.3						
	2.5	13	27.3226	56.3	7.5	13.7						
	5	13	32.8498	52.8	10.0	13.8						
d	1	18	19.9070	50.7	59.6	32.9	43.5	6.9	8.5	2.5	2.5	2.5
				2.5	2.5	2.5	2.5	2.5	2.5	2.5	4.7	
	2.5	22	21.4818	52.3	60.5	34.0	44.5	6.9	8.8	2.5	2.5	2.5
				2.5	2.5	2.6	2.6	2.5	2.5	2.5	4.7	
	5	27	27.9459	59.0	61.9	38.3	47.4	6.9	11.6	2.8	2.5	2.5
				2.5	2.7	3.2	3.5	2.5	2.5	4.3	5.1	

Table 2 Results for hinged parabolic arch

Case	h (m)	ite no.	W (kN)	Design variables d_i (cm), i=1, ..., nd								
a	1	12	43.0591	27.7								
	2.5	11	43.3323	27.0								
	5	11	48.9682	27.7								
b	1	11	42.4597	33.9	20.8							
	2.5	11	42.9327	32.5	21.1							
	5	10	48.5845	32.9	22.0							
c	1	12	42.2220	29.1	29.3	17.0						
	2.5	11	42.6171	26.5	29.2	16.6						
	5	11	47.9854	25.2	30.8	16.4						
d	1	12	37.7047	11.3	21.8	29.4	35.1	38.3	37.1	29.1	28.4	13.
				11.3	21.5	22.6	25.4	24.3	22.7	17.9	10.3	
	2.5	10	37.8863	10.3	20.4	28.9	33.2	38.3	34.8	29.1	28.0	10.3
				10.8	22.4	22.5	25.6	24.1	22.9	17.2	9.5	
	5	9	43.0559	10.2	20.3	29.6	34.0	40.4	33.7	31.1	22.3	10.1
				14.9	23.3	25.9	27.4	26.1	24.3	17.8	9.8	

in Fig. 4a under the load, is limited to 0.5 cm. The computed depth values for h=2.5 m are illustrated in Fig. 5a, b, c, d in detail for a clamped arch. The same process is repeated for a hinged parabolic arch, and plots are given in Fig. 6a, b, c, d. The other values of h are not demonstrated in the figures since they are similar, but compared in Tables 1 and 2.

5.2. Circular arch

The variation of the depth along the arch is computed for four different values of the height

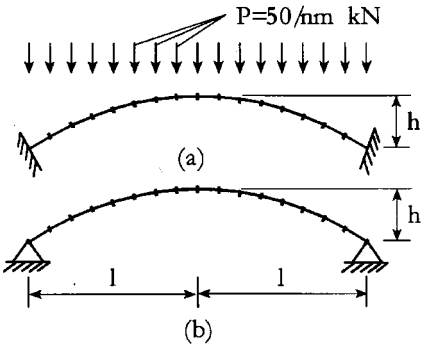

Fig. 7 Circular arch, l=10m, h=1, 2.5, 5, 7.5m (nm is the number of elements)

Table 3 Variation of the depth along a clamped circular arch

Case	h (m)	ite.no	W (kN)	Design variables (symmetric) d_i (cm), i=1, ..., nm/2+1								
d	1	9	15.43	16.3	5.4	4.6	10.4	6.2	6.6	8.6	19.8	19.3
	2.5	12	14.45	11.7	4.0	3.3	9.3	2.9	5.7	12.9	17.8	22.2
	5	213	7.92	11.9	2.5	2.8	2.5	2.5	2.5	2.7	9.8	8.8
	7.5	31	22.91	33.6	9.1	4.3	14.4	2.5	5.6	2.5	16.4	15.6

Table 4 Variation of the depth along a hinged circular arch

Case	h (m)	ite.no	W (kN)	Design variables (symmetric)							
d	1	10	17.36	3.8	8.4	9.7	11.1	5.0	6.3	15.3	19.8
	2.5	11	14.80	6.0	2.5	5.6	3.3	3.0	11.3	14.2	19.9
	5	24	13.71	4.0	11.8	8.0	11.4	2.5	2.5	2.5	14.2
	7.5	281	34.02	20.6	19.7	31.0	17.1	26.1	5.8	11.5	13.1

(Fig. 7) and the depth variation of case 2 as seen in Fig. 2. The results are given in Table 3 and 4 for clamped and hinged supports. The results for one half span are given because of symmetry. The vertical displacement at the crown is limited to 0.5 cm. The computed depth values for h=2.5 m are illustrated in Fig. 8a, b, c and Fig. 9a, b, c for clamped and hinged arches, respectively. All the cases of the depth variation as mentioned in section 3 are considered. Cases a and b give the same result (Fig. 8a, 9a), since the geometry and the loading are symmetric.

5.3. Arch with a concentrated load at mid-span

Another design example is an arch with a concentrated load of 50 kN at mid span. Both parabolic and circular arches are considered with clamped and hinged supports. The geometry and the material properties are the same as the previous examples. The depth of the arch is taken as 5 m. Only a displacement constraint, the vertical displacement at the crown, is limited to 0.5 cm. The depth variation using case 2 is computed iteratively and given in Table 5. The depths of half the arch are given since the system is symmetrical. Type 1 and type 2 represent clamped and hinged circular arches, respectively in Table 5, and type 3 shows the clamped parabolic arch.

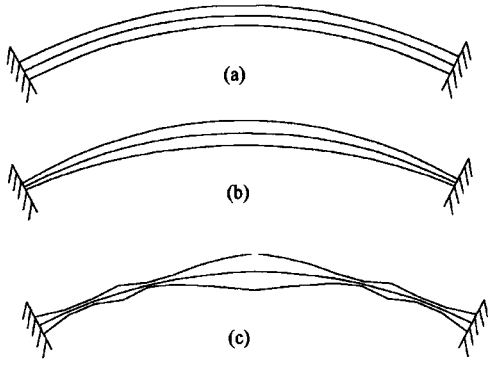

Fig. 8 Variation of the depth along a clamped circular arch

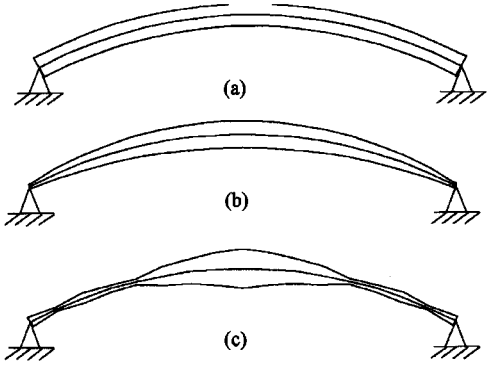

Fig. 9 Variation of the depth along a hinged circular arch

Table 5 Results for a concentrated load at mid span

arch	h (m)	ite.no	W (kN)	Design variables (symmetric) d_i (cm), i=1, ..., nm/2+1								
type 1	5	10	42.12	42.2	13.8	10.2	25.9	8.1	14.6	31.1	42.4	50.7
type 2	5	10	50.15	14.4	25.6	27.6	28.2	13.6	14.9	40.3	43.2	60.5
type 3	5	11	36.01	30.7	11.4	8.6	21.7	7.8	13.6	26.5	40.4	45.3

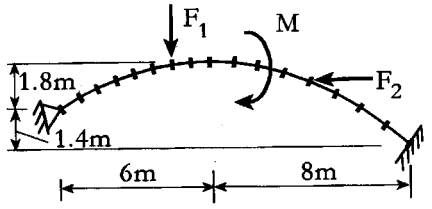

Fig. 10 A parabolic arch

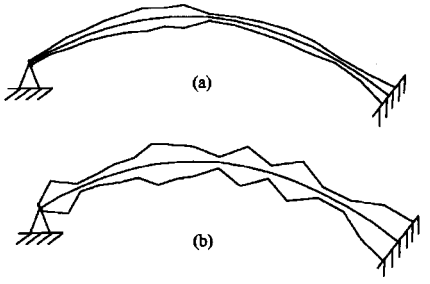

Fig. 11 Variation of the depth along the arch of Fig. 10

Table 6 Variation of the depth along arch

	ite.no	W (kN)	Average depths $t_{i,ave}$ (cm), i=1, ... , nm							
Δ=5 cm	18	7.1676	2.50	4.03	5.59	6.58	8.47	10.37	10.26	10.32
ϕ=0.1 rad			7.38	3.55	4.69	5.75	6.03	4.51	3.83	7.60
Δ=0.5 cm	540	14.5888	10.91	11.10	4.95	7.32	9.24	14.97	18.66	15.73
ϕ=0.1 rad			10.16	12.62	13.15	13.63	13.18	6.33	13.44	22.13

5.4. Parabolic arch

As a last example a parabolic arch with supports at different level is solved for two

displacement constraints. The geometric properties are shown in Fig. 10. The loads are F_1=50 kN, F_2=10 kN, M=20 kN.m. The material properties are the same as the previous examples. The vertical displacement at the crown, and the rotation of the node where M acts are desired not to exceed 5 cm, and 0.1 rad., respectively. The same calculation is repeated for the displacement constraint of 0.5 cm instead of 5 cm. The depths for this problem are computed using Eq. (11) for Case d of section 3, and the results are given in Table 6. The lower bound of the design variables is taken as 2.5 cm. The variation of the depth along the arch is plotted and illustrated in Fig. 11.a and b for each displacement constraint.

6. Conclusions

The optimality criteria approach is applied to the optimum design of the arches. Three types of constraints such as displacement, stress and minimum depth of the cross section are considered. One of these constraints has become active to evaluate the arch for minimum weight. The variation of the depth of each element becomes proportional to the bending moments if the stress constraints are active. It is observed that the weight of the arch becomes minimum when the depth of each finite segment is calculated independent of the other elements. The variation of the cross section along the arch will be different for different loading for the same arch. It is practically very important to consider every kind of loading and to find only one common optimum variation of cross section that responds to all kinds of loading and to be used during construction. The method presented in this study can be improved for this purpose.

References

Arbabi, F. (1991), *Structural Analysis and Behavior*, McGraw Hill.

Bensalem, A., Sibbald, A. and Fairfield, C.A. (1998), "The use of dynamic characteristics for the optimal design of arches", *Comp. & Struct.* **68**(5), 461-472.

Cook, R.D., Malkus, D.S. and Plesha, M.E. (1989), *Concepts and Applications of Finite Element Analysis*, John Wiley & Sons, Canada.

Ding, Y. (1986), "Shape optimization of structures: A literature survey", *Comp. & Struct.* **24**(6), 985-1004.

Haftka, R.T., Gurdal, Z. and Kamat, M.P. (1990), *Elements of Structural Optimization*, Kluwer Academic Publishers.

Hayalioglu, M.S. and Saka, M.P. (1992), "Optimum design of geometrically nonlinear elastic-plastic steel frames with tapered members", *Comp. & Struct.* **44**(4), 915-924.

Marquis, J.P. and Wang, T.M. (1989), "Stiffness matrix of parabolic beam element", *Comp. & Struct.* **31**(6), 863-870.

No, M. and Aguinagalde, J.M. (1987), "Finite element method and optimality criterion based structural optimization", *Comp. & Struct.* **27**(2), 287-295.

Saka, M.P. and Hayalioglu, M.S. (1991), "Optimum design of geometrically nonlinear elastic-plastic steel frames", *Comp. & Struct.* **38**(3), 329-344.

Saka, M.P. and Ulker, M. (1992), "Optimum design of geometrically nonlinear space trusses", *Comp. & Struct.* **42**(3), 289-299.

Tadjbakhsh, I.G. (1981), "Stability and optimum design of arch-type structures", *Int. J. Solids & Struct.* **17**, 565-574.

Tin-Loi, F. (1992), "Optimal plastic design of arches", *Comp. & Struct.* **43**(4), 675-679.

Evaluation of structural dynamic responses by stochastic finite element method

Q.S. Li†, J.Q. Fang‡ and D.K. Liu‡†

Department of Building and Construction, City University of Hong Kong
Tat Chee Avenue, Kowloon, Hong Kong

Abstract. The uncertainties associated with structural parameters and dynamic loading are identified and discussed. Structural parametric uncertainties are treated as random variables and dynamic wind load is simulated as a random process. Dynamic wind-induced responses of structures with parametric uncertainties are investigated by using stochastic finite element method. The formulas for structural dynamic reliability analysis considering the randomness of structural resistance and loading are proposed. Two numerical examples of high-rise structures are presented to illustrate the proposed methodology. The calculated results demonstrate that the variation in structural parameters indeed influences the dynamic response and the first passage probability evaluation of structures.

Key words: dynamic response; finite element method; uncertainty; dynamic reliability.

1. Introduction

Most structures have complex geometrical and material properties and are subjected to complex stochastic environment conditions. The uncertainties in the properties of material, structural damping, geometric parameters and boundary conditions etc. may induce statistical variation in the eigenvalues and eigenvectors and consequently the dynamic response may be affected. Therefore, a realistic analysis and design of structural systems with parametric uncertainties and subjected to stochastic dynamic excitations should take into account for the uncertainties arising from both structural properties and dynamic excitation simultaneously in a consistent and rational manner. However, the uncertainties associated with structural parameters are not usually considered in evaluation of random dynamic response of structures. More work is thus required to study dynamic response of structures with uncertain parameters.

As the name suggests, the stochastic finite element method (SFEM) combines the best features of the finite element methods and the stochastic analysis. Stochastic finite element method has recently become an active area of research. However, it is worth noting that the stochastic finite element method has been mainly applied in structural static analysis and eigenproblems over the last decade (e.g., Spanos and Ghanem 1989, Vanmarcke and Grigoriu 1983). The evaluation of dynamic reliability of structures with parametric uncertainties subjected stochastic dynamic loads

† Assistant Professor
‡ Research Fellow
‡† Research Fellow

by SFEM has received relatively little, if any, attention in the literature in the past.

As discussed above, reliable structural design requires correct modelling of the structural parametric uncertainties and considering these uncertainties in the structural analysis. In this paper, the stochastic finite element method is applied for response analysis of structures under stochastic dynamic load actions.

The objective of this paper is to investigate wind-induced vibrations of structures with parametric uncertainties. A probability description of structural response is presented utilising the stochastic finite element method. A reliability analysis procedure is proposed in terms of upcrossing probabilities of wind-induced response. The structural lifetime reliability can be obtained from the conditional reliability through convolution with the probability density function of lifetime extreme wind speed. The probability that a particular response component of a structure will be exceeded in a specified time period can be predicted. In this manner the inherent random nature of the load, structural resistance, and the uncertainties in the description of the wind speed are accounted for. Two numerical examples are presented to illustrate the proposed methodology and the effect of the uncertainties on structural response and dynamic reliability.

2. Dynamic response of structures with parametric uncertainties

In this paper, the uncertainties associated with structural parameters are treated as random variables and dynamic wind load is simulated as a random process, and wind-induced vibrations of structures are evaluated by the stochastic finite element method. According to the probability theory, a stochastic vector $\{Y\}$ can be expressed as

$$\{Y\} = \{\bar{Y}\} + \{\alpha\} \tag{1}$$

in which $\{\bar{Y}\}=E[\{Y\}]$ is the mean of the random vector $\{Y\}$, $\{\alpha\}$ is a random vector with zero mean.

The stochastic finite element method based on the second order perturbation method has shown its accuracy and efficiency (Kareem and Sun 1990, Kleiber and Hien 1992, Li *et al.* 1993a). According to this method, a random variable or process, a random vector or field, Z, can be expressed by the second order Taylor's series expansion at mean value of α as follows:

$$Z = \bar{Z} + \sum_{i=1}^{N} Z_i^{(1)} \alpha_i + \frac{1}{2} \sum_{i=1}^{N} \sum_{j=1}^{N} Z_{ij}^{(2)} \alpha_i \alpha_j \tag{2}$$

where $\bar{Z}$ represents the mean value of Z, the superscripts (1) and (2) denote the first and second derivatives of Z with respect to α, respectively, and N is the total number of the random variables considered.

The vibration equation of a multi-degree of freedom system is

$$[M]\{\ddot{X}\} + [C]\{\dot{X}\} + [K]\{X\} = \{F(t)\} \tag{3}$$

where $[M]$, $[C]$ and $[K]$ are the mass, damping and stiffness matrix, respectively. $\{F(t)\}$ is the vector of random dynamic excitations.

In the following analysis, the structural stiffness matrix $[K]$ and random displacement vector $\{X\}$ are represented by Eq. (2). If these expressions are introduced into the equation of motion (Eq. 3), we obtain the following zeroth-, first- and second-order equations for the dynamic response of the structural system.

Zeroth-order

$$[M]\{\ddot{\bar{X}}\} + [C]\{\dot{\bar{X}}\} + [\bar{K}]\{\bar{X}\} = \{F(t)\} \tag{4}$$

First-order

$$[M]\{\dot{X}_i^{(1)}\} + [C]\{\dot{X}_i^{(1)}\} + [\bar{K}]\{X_i^{(1)}\} = -[K_i^{(1)}]\{\bar{X}\} \tag{5}$$

Second-order

$$[M]\{\dot{X}_{ij}^{(2)}\} + [C]\{\dot{X}_{ij}^{(2)}\} + [\bar{K}]\{X_{ij}^{(2)}\} = -[K_{ij}^{(2)}]\{\bar{X}\} - [K_i^{(1)}]\{X_j^{(1)}\} - [K_j^{(1)}]\{X_i^{(1)}\}$$
$$(i, j = 1, 2, ..., N) \tag{6}$$

Because the dynamic load vector $\{F(t)\}$ is a random process vector, the response vectors, $\{\bar{X}\}$, $\{X_i^{(1)}\}$ and $\{X_{ij}^{(2)}\}$ are random process vectors, too. In this paper, the stochastic behaviours of structural stiffness matrix is propagated by means of the stochastic finite element method to demonstrate the methodology, which can be further refined to consider the randomness of structural damping and mass etc., if so desired.

Eqs. (4), (5) and (6) may be solved by the mode superposition method. Let

$$\{X\} = [\phi]\{y\} \tag{7}$$

where $[\phi]$ is the mode shape matrix, $\{y\}$ is the generalised co-ordinate vector which is a process vector and can be also represented by Eq. (2).
Thus, we have

$$\{\bar{X}\} = [\phi]\{\bar{y}\} \tag{8}$$

$$\{X_i^{(1)}\} = [\phi]\{y_i^{(1)}\} \tag{9}$$

$$\{X_{ij}^{(2)}\} = [\phi]\{y_{ij}^{(2)}\} \tag{10}$$

It is assumed that $[C]$ is a uncoupled damping matrix, then,

$$[\phi]^T[M][\phi] = [I] \tag{11}$$

$$[\phi]^T[C][\phi] = [\text{diag}(2\xi_j\omega_j)] = [C^*] \tag{12}$$

$$[\phi]^T[\bar{K}][\phi] = [K^*] = [\text{diag}(\omega_j^2)] \tag{13}$$

in which $[I]$ is a identity matrix.
Then substituting Eqs. (8)-(10) into Eqs. (4)-(6) and using left-handed multiplication by $[\phi]^T$ yield

$$\{\ddot{\bar{y}}\} + [C^*]\{\dot{\bar{y}}\} + [K^*]\{\bar{y}\} = \{f(t)\} \tag{14}$$

$$\{\dot{y}_i^{(1)}\} + [C^*]\{\dot{y}_i^{(1)}\} + [K^*]\{y_i^{(1)}\} = \{f_{1i}\} \tag{15}$$

$$\{\dot{y}_{ij}^{(2)}\} + [C^*]\{\dot{y}_{ij}^{(2)}\} + [K^*]\{y_{ij}^{(2)}\} = \{f_{2ij}\} \tag{16}$$

in which

$$\{f(t)\} = [\phi]^T\{F(t)\} \tag{17}$$

$$\{f_{1i}\} = -[\phi]^T[K_i^{(1)}][\bar{X}] \tag{18}$$

$$\{f_{2ij}\} = -[\phi]^T([K_{ij}^{(2)}]\{\bar{X}\} - [K_i^{(1)}]\{X_j^{(1)}\} - [K_j^{(1)}]\{X_i^{(1)}\}) \tag{19}$$

The covariance matrix of displacement response (only considering the first two orders) can be expressed as

$$R_x = R_{\bar{x}} + \sum_{i=1}^{N}\sum_{j=1}^{N} E(\alpha_i \alpha_j) R_{x^{(1)}}(X_i^{(1)}, X_j^{(1)}) + \frac{1}{2}\sum_{i=1}^{N}\sum_{j=1}^{N} E(\alpha_i \alpha_j)[R_{\bar{x}, x^{(2)}}(\bar{X}, X_{ij}^{(2)}) + R_{x^{(2)}, \bar{x}}(X_{ij}^{(2)}, \bar{X})] \tag{20}$$

in which

$$R_{\bar{x}} = E[\{\bar{X}\}\{\bar{X}\}^T] \tag{21}$$

$$R_{x^{(1)}}(X_i^{(1)}, X_j^{(1)}) = E(\{X_i^{(1)}\}\{X_j^{(1)}\}^T] \tag{22}$$

$$R_{\bar{x}, x^{(2)}}(\bar{X}, X_{ij}^{(2)}) = E[\{\bar{X}\}\{X_{ij}^{(2)}\}^T] \tag{23}$$

$$R_{x^{(2)}, \bar{x}}(X_{ij}^{(2)}, \bar{X}) = E[\{X_{ij}^{(2)}\}\{\bar{X}\}^T] \tag{24}$$

If spectral analysis in the frequency domain is applied, Eq. (20) can be rewritten as

$$[S_x(\omega)] = [S_{\bar{x}}(\omega)] + \sum_{i=1}^{N}\sum_{j=1}^{N} E(\alpha_i \alpha_j)[S_{x^{(1)}}(X_i^{(1)}, X_j^{(1)}, \omega)] + \frac{1}{2}\sum_{i=1}^{N}\sum_{j=1}^{N} E(\alpha_i \alpha_j)\{[S_{\bar{x}, x^{(2)}}(\bar{X}, X_{ij}^{(2)}, \omega)] + [S_{x^{(2)}, \bar{x}}(X_{ij}^{(2)}, \bar{X}, \omega)]\} \tag{25}$$

Using the matrix form, the spectral density of $\bar{y}$ can be expressed as

$$[S_{\bar{y}}(\omega)] = [H^*(\omega)][S_f(\omega)][H(\omega)] \tag{26}$$

in which $H_j(\omega)$ is the mechanical admittance function, it can be determined by use of Eq. (14),

$$[H(\omega)] = \text{diag}\{H_j(\omega)\}] \tag{27}$$

Similarly, it can be derived from Eq. (17) that

$$[S_f(\omega)] = [\phi]^T[S_F(\omega)][\phi] \tag{28}$$

From Eq. (8), we can obtain

$$[S_{\bar{X}}(\omega)] = [\phi][S_{\bar{y}}(\omega)][\phi]^T = [\phi][H^*(\omega)][\phi]^T[S_F(\omega)][\phi][H(\omega)][\phi]^T \tag{29}$$

The second term, $S_{X^{(1)}}(X_i^{(1)}, X_j^{(1)}, \omega)$ in Eq. (25) can be similarly derived from Eq. (18) as

$$\begin{aligned}[S_{X^{(1)}}(X_i^{(1)}, X_j^{(1)}, \omega)] &= [\phi][S_{y^{(1)}}(y_i^{(1)}, y_j^{(1)}, \omega)][\phi]^T = [\phi][H^*(\omega)][S_{f_1}(f_{1i}, f_{1j}, \omega)][H(\omega)][\phi]^T \\ &= [\phi][H^*(\omega)][\phi]^T[K_i^{(1)}][S_{\bar{X}}(\omega)][K_j^{(1)}]^T[\phi][H(\omega)][\phi]^T\end{aligned} \tag{30}$$

Similarly, $S_{\bar{X}, X^{(2)}}(\bar{X}, X_{ij}^{(2)}, \omega)$ can be also derived as

$$[S_{\bar{X}, X^{(2)}}(\bar{X}, X_{ij}^{(2)}, \omega)] = [\phi][S_{\bar{y}, y^{(2)}}(\bar{y}, y_{ij}^{(2)}, \omega)][\phi]^T = [\phi][H^*(\omega)][S_{f, f_2}(f, f_{2ij}, \omega)][H(\omega)][\phi]^T \tag{31}$$

Using Eqs. (17) and (19) leads to,

$$[S_{f, f_2}(f, f_{2ij}, \omega)] = -[S_{f, \bar{X}}(\omega)][K_{ij}^{(2)}]^T[\phi] - [S_{f, X^{(1)}}(f, X_j^{(1)}, (\omega)][K_i^{(1)}]^T[\phi]$$

$$-[S_{f,X^{(1)}}(f, X_i^{(1)}, \omega)][K_j^{(1)}]^T[\phi] \tag{32}$$

in which

$$[S_{f,\bar{X}}(\omega)] = [S_{f,\bar{y}}(\omega)][\phi]^T = [S_f(\omega)][H(\omega)][\phi]^T = [\phi]^T[S_F(\omega)][\phi][H(\omega)][\phi]^T \tag{33}$$

$$[S_{f,X^{(1)}}(f, X_j^{(1)}, \omega)] = [S_{f,y^{(1)}}(f, X_j^{(1)}, \omega)][\phi]^T = [S_{f,f_{1i}}(f, f_{1i}, \omega)][H(\omega)][\phi]^T$$
$$= -[S_{f,\bar{X}}(\omega)][K_i^{(1)}]^T[\phi][H(\omega)[\phi]^T = -[\phi]^T[S_F(\omega)][\phi][H(\omega)][\phi]^T[K_i^{(1)}]^T[\phi][H(\omega)][\phi]^T \tag{34}$$

The characteristic equation is given by

$$([K] - \lambda[M])\{\phi\} = 0 \tag{35}$$

Solving the characteristic equation yields the natural frequencies and the corresponding mode shapes. As discussed above, the stiffness of structures is represented by a random variable field in this paper, the natural frequencies and mode shapes of the structures are also random variables. Let

$$\lambda = \bar{\lambda} + \sum_{i=1}^{N} \lambda_i^{(1)} \alpha_i + \frac{1}{2} \sum_{i=1}^{N} \sum_{i=1}^{N} \lambda_{ij}^{(2)} \alpha_i \alpha_j \tag{36}$$

and

$$\{\phi\} = \{\bar{\phi}\} + \sum_{i=1}^{N} \{\phi\}_i^{(1)} \alpha_i + \frac{1}{2} \sum_{i=1}^{N} \sum_{i=1}^{N} \{\phi\}_{ij}^{(2)} \alpha_i \alpha_j \tag{37}$$

Substituting Eq. (36) and Eq. (37) into Eq. (35) leads to,

$$([\bar{K}] + \sum_{i=1}^{N} [K_i^{(1)}]\alpha_i + \frac{1}{2} \sum_{i=1}^{N} \sum_{i=1}^{N} [K_{ij}^{(2)}] \alpha_i \alpha_j - \bar{\lambda}\,[M] - \sum_{i=1}^{N} [M]\,\alpha_i \lambda_i^{(1)} -$$
$$\frac{1}{2} \sum_{i=1}^{N} \sum_{i=1}^{N} [M]\,\lambda_{ij}^{(2)} \alpha_i \alpha_j)\,(\{\bar{\phi}\} + \sum_{i=1}^{N} \{\phi_i^{(1)}\}\,\alpha_i + \frac{1}{2} \sum_{i=1}^{N} \sum_{i=1}^{N} \{\phi_{ij}^{(2)}\}\,\alpha_i \alpha_j) = \{0\} \tag{38}$$

The above equation can be rewritten as

$$([\bar{K}] - \bar{\lambda}\,[M])\{\bar{\phi}\} = 0 \tag{39}$$

$$([\bar{K}] - \bar{\lambda}\,[M])\{\phi_i^{(1)}\} = -([K_i^{(1)}] - \lambda_i^{(1)}\,[M])\{\bar{\phi}\} \tag{40}$$

$$([\bar{K}] - \bar{\lambda}\,[M])\{\phi_{ij}^{(2)}\} = -([K_{ij}^{(2)}] - \lambda_{ij}^{(2)}\,[M])\{\bar{\phi}\} - ([K_i^{(1)}] - \lambda_i^{(1)}[M])\{\phi_j^{(1)}\}$$
$$-([K_j^{(1)}] - \lambda_j^{(1)}[M])\{\phi_i^{(1)}\} \tag{41}$$

Because Eq. (39) is a deterministic equation, the eigenvalue $\bar{\lambda}_i$ and the corresponding eigenvector $\{\bar{\phi}\}_i$ can be determined directly by using conventional eigensolution procedure (e.g., Wang 1978, Li *et al.* 1994, 1996). The solutions of Eq. (40) and Eq. (41) can be found in the Appendix of this paper.

In the following analysis, for the sake of illustration, the formulation is restricted to dynamic wind loading.

If the dynamic load is wind action, and the fluctuating drag is

$$\{F(t)\} = [B]\{p(t)\} \tag{42}$$

where $[B]=[\text{diag}(C_D A_i)]$ is the product of the drag coefficient of the structure, C_D, and windward area of the structure A_i. $\{p(t)\}$ can be expressed as follows

$$\{p(t)\} = \rho[\bar{V}]\{v(t)\} \tag{43}$$

where $[\bar{V}] = [\text{diag}(\bar{V}_i)]$, $\bar{V}_i$ and $v_i(t)$ are the mean wind velocity and the fluctuating components of wind velocity, respectively, at the lumped mass point i. ρ is density of air.

The following equation can be derived from Eqs. (42) and (43)

$$[S_F(\omega)] = \rho^2[B][\bar{V}][S_v(\omega)][\bar{V}]^T[B]^T \tag{44}$$

It is assumed that each term of the matrix, $[S_v(\omega)]$, can be expressed as

$$S_{v_i,v_j}(\omega) = \rho(z_i, z_j, \omega)\, S_v(\omega) \tag{45}$$

where $s_v(\omega)$ is the gust spectrum, and $\rho(z_i, z_j, \omega)$ is the coherence of gust, as suggested by Davenport (1962); it can be taken as,

$$\rho(z_i, z_j, \omega) = \exp\left[-\frac{4\omega|z_i - z_j|}{\pi\bar{V}}\right] \tag{46}$$

In this paper, the Davenport spectrum of wind speed is adopted,

$$s_v(\omega) = \frac{4K\bar{V}_{10}^2}{\omega}\frac{x^2}{(1+x^2)^{4/3}} \tag{47}$$

in which

$$x = \frac{600\omega}{\pi\bar{V}_{10}} \tag{48}$$

where K is the coefficient of ground roughness, $\bar{V}_{10}$ is the mean wind speed at 10m height.

The variances of displacement and velocity responses can be determined by the following equations

$$\sigma_X^2 = \int_0^\infty S_X(\omega)\, d\omega \tag{49}$$

$$\sigma_{\dot{X}}^2 = \int_0^\infty \omega^2 S_X(\omega)\, d\omega \tag{50}$$

3. Dynamic reliability analysis of structures

The structural dynamic reliability is the probability that the structure under the action of random dynamic loads will fulfil its design purpose during a specified period.

If it is assumed that the lifetime of a structure is n years, in general, n is taken as 50, and the probability density function of maximum wind velocity in the n years is $f(\bar{v})$ which can be derived from a statistical analysis of successive years of climatological data, then, the reliability of the structure in its lifetime can be expressed as

$$P_s = \int_0^\infty P(S \le R \mid \bar{V} = \bar{v})\, f(\bar{v})\, d\bar{v} \tag{51}$$

in which S is the structural response quality of interest, R is the corresponding structural resistance. $P(S \le R \mid \bar{V} = \bar{v})$ is called the conditional reliability of the structure given $\bar{V} = \bar{v}$.

Eq. (51) can be written in a discrete form so that it is convenient to be calculated.

$$P_s = \sum_k P(S \le R \mid \bar{V} = \bar{v})[F(\bar{v}_k) - F(\bar{v}_{k-1})] \tag{52}$$

where $F(\bar{v})$ is probability distribution function of the maximum wind speed in the n years.

Analysis of data at various locations with well-behaved wind climates has suggested that the extreme value Type I distribution in general provides a good fit to the extreme yearly wind speed (Simiu 1976, Li 1986, 1988, 1990). A maximum probability plot correlation coefficient criterion has been employed in a study (Kareem and Hseih 1986) for modelling annual extreme winds and also confirm Simiu's conclusion.

Assuming that yearly maximum wind speeds over a period of n years are independent, the PDF of the n years extreme wind speed can be expressed as

$$f(\bar{v}) = na \exp\{-(\bar{v} - a)b - n \exp[-(\bar{v} - a)b]\} \tag{53}$$

in which parameters a and b can be determined from a large sample of annual extreme mean wind speed data by the method of moments.

A typical upcrossing problem for dynamic reliability is illustrated in Fig. 1. If the deterioration of structural resistance with time is considered, then, the reliability bound is a function of time t. The upcrossing rate per unit time, $v(t)$ can be expressed as

$$v(t) = \int_0^\infty v_r(t)\, f_R(r)\, dr \tag{54}$$

where (Rice 1944)

$$v_r(t) = \int_r^\infty (\dot{s} - \dot{r})\, f_{s,\dot{s}}(r, \dot{s})\, d\dot{s} \tag{55}$$

in which $v_r(t)$ is the upcrossing rate per unit time for the barrier $R=r$ with slope $\dot{r}$, $f_R(r)$ is the

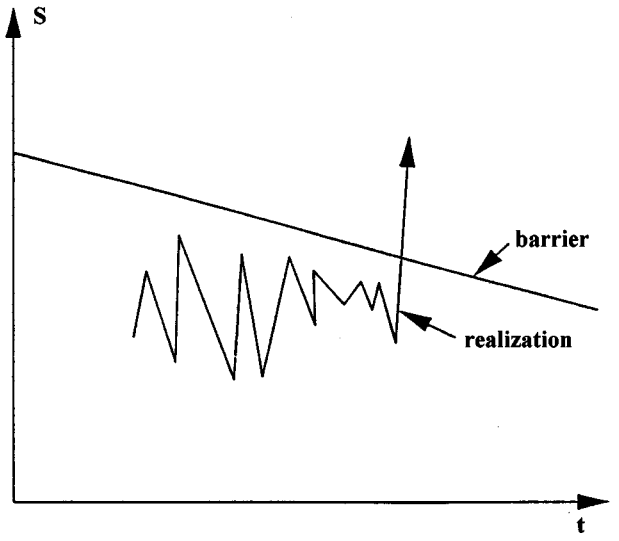

Fig. 1 Typical upcrossing problem for dynamic reliability analysis

probability density function of structural resistance. $\dot{s}$ is a state variable of $\dot{S}(t)$ which is the derivative process of $S(t)$ with respect to t.

If it is assumed that $S(t)$ is a Normal stationary process with zero mean, then, $S(t)$ and $\dot{S}(t)$ are independent Normal stationary process and can be estimated by the procedure presented in the preceding section, the joint probability density function of $S(t)$ and $\dot{S}(t)$ is

$$f_{s,\dot{s}}(s,\dot{s}) = \frac{1}{2\pi\sigma_s\sigma_{\dot{s}}}\exp\left[-\frac{1}{2}\left(\frac{s^2}{\sigma_s^2}+\frac{\dot{s}^2}{\sigma_{\dot{s}}^2}\right)\right] \tag{56}$$

Substituting Eq. (56) into Eq. (55) gives

$$v_r(t) = \frac{A}{2\pi}\frac{\sigma_{\dot{s}}}{\sigma_s}\exp\left(-\frac{r^2}{2\sigma_s^2}\right) \tag{57}$$

in which

$$A = \exp\left(\frac{-\dot{r}^2}{2\sigma_{\dot{s}}^2}\right) - \sqrt{2\pi}\frac{\dot{r}}{\sigma_{\dot{s}}}\phi\left(\frac{-\dot{r}}{\sigma_{\dot{s}}}\right) \tag{58}$$

and $\phi(.)$=the standardised Normal distribution function.

If structural resistance obeys the Normal distribution, that is

$$f_R(r) = \frac{1}{2\pi\sigma_R}\exp\left[-\frac{(r-\bar{r})^2}{2\sigma_R^2)}\right] \tag{59}$$

then

$$P(S \le R \mid \bar{V} = \bar{v}) = \exp\left\{-\frac{A\,\tau\sigma_{\dot{s}}}{2\pi\sqrt{\sigma_s^2+\sigma_R^2}}\exp\left[-\frac{\bar{r}^2}{2(\sigma_s^2+\sigma_R^2)}\right]\right\} \tag{60}$$

in which τ is the duration of dynamic response considered; in general, for wind loading, τ=10 min.

If the upper and lower bounds of structures for dynamic reliability analysis are considered, then,

$$P(S \le R \mid \bar{V} = \bar{v}) = \exp\left\{-\frac{A\,\tau\sigma_{\dot{s}}}{2\pi\sqrt{\sigma_s^2+\sigma_{R_1}^2}}\exp\left[-\frac{\bar{r}_1^2}{2(\sigma_2^2+\sigma_{R_2}^2)}\right] - \frac{A\,\tau\sigma_{\dot{s}}}{2\pi\sqrt{\sigma_s^2+\sigma_{R_2}^2}}\exp\left[-\frac{\bar{r}_2^2}{2(\sigma_s^2+\sigma_{R_2}^2)}\right]\right. \tag{61}$$

where $\bar{r}_1, \bar{r}_2$ and $\sigma_{R_1}, \sigma_{R_2}$ are the mean values and standard deviations of R_1 (the upper bound) and R_2 (the lower bound), respectively.

If.R_1=R_2=R (symmetric bound), Eq. (61) becomes

$$P(S \le R \mid \bar{V} = \bar{v}) = \exp\left\{-\frac{A\,\tau\sigma_{\dot{s}}}{\pi\sqrt{\sigma_s^2+\sigma_R^2}}\exp\left[-\frac{\bar{r}^2}{2(\sigma_s^2+\sigma_R^2)}\right]\right\} \tag{62}$$

If the deterioration of structural resistance is not considered, that is $\dot{r}=0$, it can be obtained from Eq. (58) that $A=1$.

4. Numerical Example 1

Wuhan T.V. Tower located in Wuhan City, P.R. China is analysed here as a numerical example for the present study. As shown in Fig. 2, this tower consists of tower base, tower body, tower building and a wireless mast. The main structure of the T.V. Tower is a reinforced concrete cone shell with the diameter of the cone varying linearly along the height. Its external base section diameter section is 16m and that of the top section is 3.9m. In the analysis of wind-induced vibration of the tower, the structure is treated as an 18 lumped mass system. Li (1995) investigated free vibration of the tower. The geometric dimension, mass and stiffness distributions of the Wuhan T.V. tower are listed in Table 1.

Li *et al.* (1993b) conducted a detailed statistical analysis of successive years of climatological data for the region of Wuhan, P.R. China. They obtained the probability distribution function

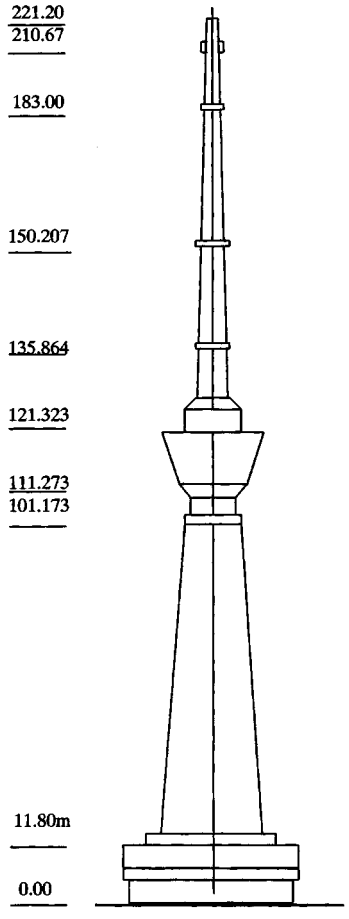

Fig. 2 Wuahn T.V. Tower

(PFD) of the maximum local wind speed (the averaging time is ten minutes) in the n years [$F(\bar{v})$], which can be adopted for the present dynamic reliability analysis for this T.V. tower. They also found that strong wind in Wuhan City usually occurs in NNE-NE direction, and the corresponding $F(\bar{v})$ in NNE-NE direction was obtained by Li *et al.* (1993b).

As suggested by Li *et al.* (1993b), the wind velocity at the location of the tower is taken as

$$\bar{V}(z) = \bar{V}(10)\left(\frac{z}{10}\right)^{0.16} \tag{63}$$

in which $\bar{V}(z)$ is the mean wind speed at height z.

In the dynamic reliability analysis for the T.V. tower, the top displacement response of this tower is taken as the critical index; Davenport's wind speed spectrum is adopted and the coefficient of ground roughness, K, is taken as 0.003. The calculated results of the dynamic reliability analysis are shown in Fig. 3, in which curve 1 represents the results computed by the Monte Carlo simulation; curve 2 and curve 3 correspond to the dynamic reliability results calculated based on the PDF of the maximum local wind speed for all the wind directions and for NNE-NE direction only, respectively. It can be seen that the calculated results by the proposed procedure are in good agreement with the simulated data by the Monte Carlo method. In particular, when n<10 years, the three sets of data are almost identical, when n=100 years, the difference between them is less than 10 per cent, demonstrating the good applicability of the proposed procedure for the evaluation of structural dynamic reliability.

Table 1. The geometric dimension, mass and stiffness distributions of the T.V. Tower

Lumped Mass No.	Height m	Diameter m	Mass Kg	Stiffness $EJ_i \times 10^7$ KN.m^2
0	0	16		
1	4.975	15	72,571	28,440
2	17.412	12.5	66,739	26,320
3	22.387	11.5	60,849	24,157
4	27.377	10.875	54,192	17,064
5	29.876	10.75	59,317	22,388
6	32.375	10.625	41,658	9,582
7	34.874	10.5	57,256	24,844
8	104.853	7.0	37,208	8,622
9	108.853	7.0	20,735	1,426
10	110.803	7.6	20,735	1,428
11	114.253	7.0	37,935	2,847
12	133.653	7.0	20,735	1,428
13	138.622	5.88	20,735	1,428
14	139.864	5.6	20,281	837
15	142.303	4.5	14,314	374
16	164.203	4.5	14,324	374
17	156.685	3.9	9,759	196
18	187	3.9	9,759	196

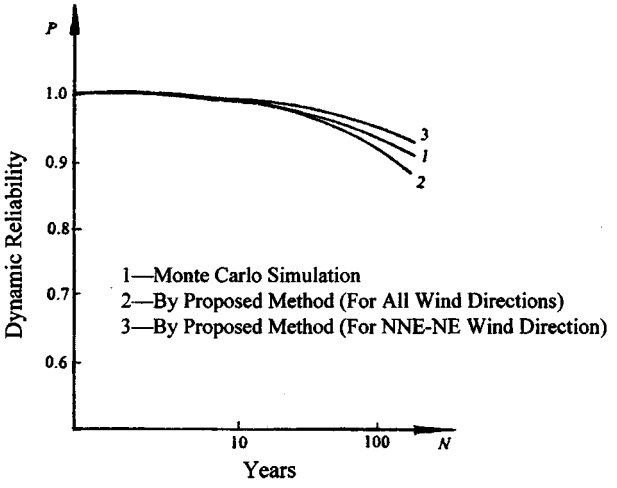

Fig. 3 Dynamic reliability of Wuhan T.V. Tower

5. Numerical Example 2

In the last numerical example, an overall good agreement between the results calculated by the proposed procedure and those simulated by the Monte Carlo method has provided confidence on the proposed computational method and computer programme. Another numerical example utilising a chimney 60m high modelled as a lumped-mass system is analysed here to study the effect of the variation in structural parameters on the structural dynamic reliability. This stack is divided into 8 sections for computation purpose. The Young's modulus of the chimney is 3000 MPa (the coefficient of variation,V=0.01). The structural parameters are listed in Table 2. The top displacement response of this chimney is taken as the critical index in dynamic reliability analysis. The dynamic response of this chimney, considering the randomness of structural stiffness and wind loading, is evaluated according to the procedures proposed in the preceding sections. The results of dynamic reliability analysis of this high-rise structure under wind action computed by the present method are given in Table 3. The effects of structural critical damping ratio ξ and resistance represented by the permissible displacement which is a random variable on dynamic reliability of this structure can be clearly seen through the calculated results presented in Table 3. It is clear that the dynamic reliability of this structure becomes larger as the structural damping and resistance increase.

Table 4 presents the effect of the variation of the structural resistance on the dynamic reliability of this stack. It is clear that the larger the structural resistance variation is, the lower its dynamic reliability is. In particular, this effect becomes more pronounced at large value of V. It should be noted that the variation of structural resistance is inevitable during a long period (e.g., 50 or 100 years) and it is random in nature. The calculated results of this chimney show that the variation in

Table 2 Structural parameters

Section length (meter)	5.0	8.0	7.0	7.5	7.5	7.5	7.5	10.0
Outside diameter (meter)	5.03	4.61	4.31	4.02	3.72	3.42	3.12	2.77
Section weight (KN)	1112	1307	944	899	815	623	577	520

Table 3 The effects of damping ratio ξ and structural resistance (coefficient of variation V=0) on structural dynamic reliability

$\bar{r}$	ξ	10 (year)	20 (year)	30 (year)	40 (year)	50 (year)
H/100	0.02	0.9976	0.9967	0.9954	0.9937	0.9926
H/100	0.03	0.9984	0.9978	0.9971	0.9968	0.9963
H/200	0.02	0.8872	0.7880	0.7700	0.6216	0.5522
H/200	0.03	0.9443	0.8928	0.8442	0.7981	0.7543

Note: H is the chimney height (60m).

Table 4 The effects of structural resistance variation on the structural dynamic reliability

$\bar{r}$	ξ	P (50 Years)
H/100, V=0	0.02	0.9926
H/100, V=0.11	0.02	0.9912
H/100, V=0.25	0.02	0.9322

structural parameters indeed influence the first passage probability of this structure. These parameters such as the structural resistance should be treated as random variables in the evaluation of structural dynamic reliability.

6. Conclusions

In this paper, structural parametric uncertainties and structural resistance were treated as random variables, and dynamic wind load was considered as a random process. Structural dynamic responses under the action of stochastic wind loads are evaluated by the stochastic finite element method. The formulas for structural dynamic reliability analysis considering the randomness of structural resistance and external dynamic loading are proposed. Two numerical examples of high-rise structures are presented to illustrate the proposed methodology. The calculated results demonstrate the good applicability of the proposed procedure and that the variation in structural parameters indeed influences the structural responses and dynamic reliability.

References

Davenport, A.G. (1962), "The response of slender line-like structures to a gusty wind", *Proc. I.C.E.*, **23**, 449-472.

Kareem, A. and Hseih, J. (1986), "Reliability analysis of concrete chimneys under wind loadings", *J. Wind Engrg. & Ind. Aerodyn.*, **25**.

Kareem, A. and Sun, W.J. (1990), "Dynamic response of structures with uncertain damping", *Engineering Structure*, **12**, 1-8.

Kleiber, M. and Hien, T.D. (1992), "The stochastic finite element method", *John Wiley & Sons.*

Li, Q.S. (1986), "Dynamic reliability of tall buildings and high-rise structures with distributed parameters under the action of wind load", *Journal of Engineering Mechanics*, **3**(3).

Li, Q.S. (1988), "Analysis of random response and dynamic reliability of structures subjected to wind load", *Journal of Earthquake Engineering and Engineering Vibration*, **3**.

Li, Q.S. (1990), "Analysis of fuzzy random response and reliability of earthquake-resistant structures", *Chinese Journal of Applied Mechanics,* **7**(3).
Li, Q.S. (1995), "Calculation of free vibration of high-rise structures", *Asian Journal of Structural Engineering,* **1**(1), 17-25.
Li, Q.S., Cao, H. and Li, Z. (1993a), "Dynamic Response and Reliability Analysis of Random Structures", *Journal of Applied Mathematics and Mechanics,* **14**(10), 983-991.
Li, Q.S., Cao, H. and Li, G.Q. (1993b), "Dynamic reliability of Wuhan T.V. Tower under the action of wind load", *Proceedings of the Third Asia-Pacific Symposium on Wind Engineering,* **1**, Hong Kong, December, 391-196.
Li, Q.S., Cao, H. and Li, G.Q. (1994), "Analysis of free vibrations of tall buildings", ASCE, *Journal of Engineering Mechanics,* **120**(9), 1861-1876.
Li, Q.S., Cao, H. and Li, G.Q. (1996), "Static and dynamic analysis of straight bars with variable cross-section", *International Journal of Computers & Structures,* **59**(6), 1185-1191.
Spanos, P.D. and Ghanem, R. (1989), "Stochastic finite element expansion for random media", *ASCE, Journal of Engineering Mechanics,* **115**, 1035-1053.
Simiu, E. (1976), "The probability distributions of extreme wind speeds", *J. Struc. Div., ASCE,* **107**(ST9).
Rice, S.O. (1944), "Mathematical analysis of random noise", *Bell System Tech. Journal,* **23**, 282-332.
Vanmarcke, E.H. and Grigoriu, M. (1983), "Stochastic finite element analysis of simple beam", *ASCE, Journal of Engineering Mechanics,* **109**, 1203-1214.
Wang, G.Y. (1978), "Vibration of building and structures", Science and Technology Press.

Appendix

When a structural stiffness matrix is a stochastic matrix, the natural frequency and mode shape of the structure are thus random variables. In this case, the characteristic equations can be expressed as

$$([\bar{K}]-\bar{\lambda}[M])\{\bar{\phi}\}=0 \tag{A.1}$$

$$([\bar{K}]-\bar{\lambda}[M])\{\phi_i^{(1)}\}=-([K_i^{(1)}]-\lambda_i^{(1)}[M])\{\bar{\phi}\} \tag{A.2}$$

$$([\bar{K}]-\bar{\lambda}[M])\{\phi_{ij}^{(2)}\}=-([K_{ij}^{(2)}]-\lambda_{ij}^{(2)}[M])\{\bar{\phi}\}-([K_i^{(1)}]-\lambda_i^{(1)}[M])\{\phi_j^{(1)}\}-([K_j^{(1)}]-\lambda_j^{(1)}[M])\{\phi_i^{(1)}\} \tag{A.3}$$

Because Eq. (A.1) is a deterministic equation, the eigenvalues $\bar{\lambda}_i$ and the corresponding eigenvectors $\{\bar{\phi}\}_i$, (i=1, 2, ...) can be determined by conventional eigensolution procedures. According to the orthogonality properties of mode shapes we assume

$$\{\bar{\phi}\}^T[M]\{\bar{\phi}\}=I \tag{A.4}$$

Using the symmetry behaviour of matrix yields the transposition of Eq. (A.1) as follows

$$\{\bar{\phi}\}^T([\bar{K}]-\bar{\lambda}[M])=\{0\}^T \tag{A.5}$$

Letting the left-hand of Eq. (A.2) multiplication by $\{\bar{\phi}\}^T$ and according to Eq. (A.5) lead to

$$\{0\}=-\{\bar{\phi}\}^T([K_i^{(1)}]-\lambda_i^{(1)}[M])\{\bar{\phi}\} \tag{A.6}$$

then

$$\lambda_i^{(1)}=\{\bar{\phi}\}^T[K_i^{(1)}]\{\bar{\phi}\} \tag{A.7}$$

Because the coefficient determinant of $\{\phi_i^{(1)}\}$ is equal to zero, we can not directly find $\{\phi_i^{(1)}\}$ in Eq. (A.2). Thus, it is necessary to make the following assumption.

$$\{\bar{\phi}\}^T[M]\{\phi_i^{(1)}\}=0 \tag{A.8}$$

Then, Eq. (A.2) and Eq. (A.8) can be unified as

$$\begin{bmatrix} [\bar{K}] - \bar{\lambda}[M] \\ \{\bar{\phi}\}^T[M] \end{bmatrix} \{\phi_i^{(1)}\} = - \begin{bmatrix} [k_i^{(1)}] - \lambda_i^{(1)}[M] \\ 0 \end{bmatrix} \{\bar{\phi}\} \tag{A.9}$$

or

$$[C_1]\{\phi_i^{(1)}\} = [D_1]\{\bar{\phi}\} \tag{A.10}$$

in which

$$[C_1] = \begin{bmatrix} [\bar{K}] - \bar{\lambda}[M] \\ \{\bar{\phi}\}^T[M] \end{bmatrix}, \quad [D_1] = - \begin{bmatrix} [K_i^{(1)}] - \lambda_i^{(1)}[M] \\ 0 \end{bmatrix}$$

The matrix $([C_1]^T[C_1])$ is a non-singular matrix. Letting the left-hand of Eq. (A.10) multiplication by $[C_1]^T$, we can obtain

$$\{\phi_i^{(1)}\} = ([C_1]^T[C_1])^{-1}[C_1]^T[D_1]\{\bar{\phi}\} \tag{A.11}$$

The procedure of solving the eigenvalues $\lambda_{ij}^{(2)}$ and eigenvectors $\phi_{ij}^{(2)}$ of Eq. (A.3) is similar to that of Eq. (A.2). Letting left-hand multiplication by $\{\bar{\phi}\}^T$ for Eq. (A.3) yields,

$$\{\bar{\phi}\}^T[K_{ij}^{(2)}]\{\bar{\phi}\} - \lambda_{ij}^{(2)} + \{\bar{\phi}\}^T([K_i^{(1)}]\{\phi_j^{(1)}\} + [K_j^{(1)}]\{\phi_i^{(1)}\}) = 0 \tag{A.12}$$

The assumption given in Eq. (A.8) is adopted in the derivation for the above equation. From the above equation, we obtain

$$\lambda_{ij}^{(2)} = \{\bar{\phi}\}^T([K_{ij}^{(2)}]\{\bar{\phi}\} + [K_i^{(1)}]\{\phi_j^{(1)}\} + [K_j^{(1)}]\{\phi_i^{(1)}\}) \tag{A.13}$$

Similar to Eq. (A.8), the following assumption is made, that is

$$\{\bar{\phi}\}^T[M]\{\phi_{ij}^{(2)}\} + \{\phi_i^{(1)}\}^T[M]\{\phi_j^{(1)}\} = 0 \tag{A.14}$$

Eq. (A.14) and Eq. (A.3) can be unified as

$$[C_1]\{\phi_{ij}^{(2)}\} = -[D_2]\{\bar{\phi}\} + [E_i]\{\phi_j^{(1)}\} + [E_j]\{\phi_i^{(1)}\} \tag{A.15}$$

where

$$[D_2] = - \begin{bmatrix} [K_{ij}^{(2)}] - \lambda_{ij}^{(2)}[M] \\ 0 \end{bmatrix} \quad [E_k] = \begin{bmatrix} [K_k^{(1)}] - \lambda_k^{(1)}[M] \\ \frac{1}{2}\{\phi_k^{(2)}\}[M] \end{bmatrix} \quad (k=i \text{ or } j) \tag{A.16}$$

From Eq. (A.15) we can obtain the following equation

$$\{\phi_{ij}^{(2)}\} = ([C_1]^T[C_1])^{-1}[C_1]^T(-[D_2]\{\bar{\phi}\} + [E_i]\{\phi_j^{(1)}\} + [E_j]\{\phi_i^{(1)}\}) \tag{A.17}$$